PERGAMON

International Journal of Heat and Mass Transfer 44 (2001) 1759–1766

International Journal of HEAT and MASS TRANSFER

www.elsevier.com/locate/ijhmt

Numerical study of formation of longitudinal vortices in natural convection flow over horizontal and inclined surfaces

Ming-Han Lin *

Department of Automation Engineering, Ta-Hwa Institute of Technology, 307 Hsinchu, Taiwan, ROC

Received 17 December 1999; received in revised form 9 June 2000

Abstract

This paper presents a numerical study of the formation of longitudinal vortices in natural convection flow over horizontal and inclined plates. The criterion on the position marking on the onset of longitudinal vortices is defined in the present paper. The results show that the onset position characterized by the Grashof number depends on the Prandtl number, wave number, and the inclined angle ϕ from the horizontal. The flow is found to become more stable to the vortex mode of instability as the value of inclined angle increases, owing to a decrease in buoyancy force in the normal direction. However, the Prandtl number has a destabilizing effect on the flow. The results of the present numerical prediction show a reasonable agreement with the experimental data in the literature.

Keywords: Natural convection; Grashof number; Longitudinal vortices

1. Introduction

The problem of thermal instability in a laminar natural convection flow over horizontal and inclined plates has received attention in the heat transfer literature. The instability mechanism is due to the presence of a buoyancy force component in the direction normal to the plate surface. The appearance of longitudinal vortices was observed (e.g. [1–3], etc.). The onset and development of longitudinal vortices are of interest because of their importance to industrial applications such as chemical vapor deposition [4] and cooling of electronic packages [5,6]. It is advantageous to suppress the vortices so as to achieve uniform deposition in chemical vapor deposition processes. In contrast, it is desirable to enhance the vortices so as to induce earlier transition to turbulence and increase heat transfer from the surface in surface cooling.

There is a large body of literature on the vortex instability in natural convection flow over horizontal and inclined plates (e.g. [3,7,8], etc.). However, a quantitative agreement between theory and experiment for the onset of vortex instability of the flow under consideration is still unsatisfactory. The discrepancy between the theoretical critical Grashof number Gr_X^* and these experimental data were one to two orders in the literature. By reviewing the criteria on the onset of longitudinal vortices in boundary layer and channel flows, the experimental and numerical methods employed in the literature for determining the onset of longitudinal vortices were summarized in [9].

The attempt of this paper is to present a numerical experiment for the onset and subsequent linear development of longitudinal vortices in natural convection flow over horizontal and inclined plates. The experimental criteria proposed by Hwang and Lin [9] on the onset of longitudinal vortices were employed in the present study. The governing parameters on the onset of longitudinal vortices are the Prandtl number, the wave number a, the inclined angle ϕ from the horizontal, and the Grashof number. In the computation, the Prandtl number is 0.7 (for air) and 7.0 (for water), the inclined angle from the horizontal $\phi = 0°$, 5°, 10°, 15°, 20°, 30°, 45°, 60°, and 70°, the magnitudes of imposed initial

* Tel.: +886-3-5927700; fax: +886-03-5921047.
E-mail address: aemhlin@et4.thit.edu.tw (M.-H. Lin).

0017-9310/01/$ - see front matter
PII: S0017-9310(00)00213-1

Nomenclature

a'	dimensional wave number, $a' = 2\pi/\lambda$
a	dimensionless wave number, $a = a'L/Gr_L^{1/5}$
F	velocity, pressure or temperature function
f	reduced stream function, $\psi(v/Gr_X^{1/5})^{-1}$
Gr_X	local Grashof number, $Gr_X = (g\beta(T_w - T_\infty)\,X^3)/v^2$
h	local heat transfer coefficient
p', p	dimensional and dimensionless pressures, $p' = \rho v^2 Gr_L^{4/5} p/L^2$
Pr	Prandtl number, v/α
Nu_X	local Nusselt number, hX/k
T	temperature (K)
t', t	dimensional and dimensionless perturbation temperatures, $t' = (T_w - T_\infty)t$
t^0	initial constant perturbation temperature at $x = 0$
U, V, W	dimensional velocity components (m/s)
u, v, w	dimensionless perturbation velocity components
u', v', w'	perturbation velocity components
X, Y, Z	Cartesian coordinates (m)
x, y, z	dimensionless Cartesian coordinates as defined in (14)

Greek symbols

δ	boundary layer thickness (m)
η	similarity variable, $YGr_X^{1/5}/X$
θ_b	dimensionless basic temperature, $(T - T_\infty)/(T_w - T_\infty)$
λ	wavelength in the Z-direction (m)
v	kinematic viscosity of the fluid (m^2/s)
ξ	vorticity function in the X-direction defined in (15) (1/s)
ψ	stream function (m^2/s)

Superscript

$*$	onset position

Subscripts

b	basic flow quantity
p	perturbation quantity
w	wall condition
X	local coordinate
∞	free stream condition

disturbance temperature $t^0 = 10^{-4}$, and the flat plate Grashof number $Gr_L = 10^8$.

2. Theoretical analysis

Consider a laminar natural convection flow over horizontal and inclined heated plates, as shown in Fig. 1. The acute angle of inclination from the horizontal is ϕ. The physical Cartesian coordinates are chosen such that X measures the streamwise distance from the leading edge of the plate, Y is the distance normal to the plate, and Z is in the transverse direction. The streamwise and normal velocity components are U_b and V_b. The governing boundary layer equations for constant-property fluids under the Boussinesq approximation can be written as

$$\frac{\partial U_b}{\partial X} + \frac{\partial V_b}{\partial Y} = 0, \tag{1}$$

$$U_b\frac{\partial U_b}{\partial X} + V_b\frac{\partial U_b}{\partial Y} = v\frac{\partial^2 U_b}{\partial Y^2} + g\beta\cos\phi\,\frac{\partial}{\partial X}\int_Y^\infty (T_b - T_\infty)\,dY + g\beta(T_b - T_\infty)\sin\phi, \tag{2}$$

$$U_b\frac{\partial T_b}{\partial X} + V_b\frac{\partial T_b}{\partial Y} = \alpha\frac{\partial^2 T_b}{\partial Y^2}, \tag{3}$$

where T_w is the surface temperature and T_∞ is the free-stream temperature.

Next, one introduces the following dimensionless variables and parameters:

$$X = Lx, \quad Y = LGr_L^{-1/5}y,$$

$$U_b = \frac{v}{L}Gr_L^{2/5}\bar{u}, \quad V_b = \frac{v}{L}Gr_L^{1/5}\bar{v}, \quad \theta_b = \frac{T_b - T_\infty}{T_w - T_\infty}, \tag{4}$$

$$\eta = YGr_X^{1/5}/X, \quad f(X,\eta) = \psi\left(v/Gr_X^{1/5}\right)^{-1},$$

where $f(X,\eta)$ is the reduced stream function. The basic flow equations (1)–(3) transformed from (X, Y) into the (X,η) plane are:

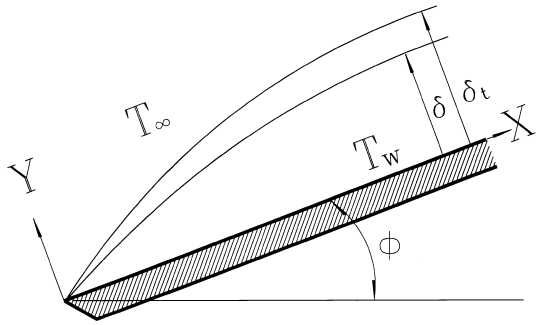

Fig. 1. Physical configuration and coordinate system.

$$f''' + \left(\frac{3}{5}f + x\frac{\partial f}{\partial x}\right)f'' - xf'\frac{\partial f'}{\partial x} - \frac{1}{5}f'^2 = -Gr_L^{1/5}x^{3/5}\theta_b \sin\phi - \left[\frac{2}{5}\int_\eta^\infty \theta_b \, d\eta + \frac{2}{5}\eta\theta_b + x\int_\eta^\infty \frac{\partial\theta_b}{\partial x}\, d\eta\right]\cos\phi, \quad (5)$$

$$\theta_b'' + \left(\frac{3}{5}f + x\frac{\partial f}{\partial x}\right)Pr\,\theta_b' - xPrf'\frac{\partial\theta_b'}{\partial x} = 0. \quad (6)$$

The boundary conditions are as follows:

$$\begin{aligned} &f(X,0) = f'(X,0) = \theta_b(X,0) - 1 = 0,\\ &f'(X,\infty) = \theta_b(X,\infty) = 0. \end{aligned} \quad (7)$$

In Eqs. (5)–(7), the primes denote the partial derivatives with respect to η and Pr is the Prandtl number.

2.1. Perturbation equations

In the region near or upstream of the onset position x^*, the disturbances of the longitudinal vortex type are small and the nonlinear terms in the momentum and energy equations may be linearized. Furthermore, in experiments [1–3], etc. 'stationary' longitudinal vortex rolls have been found tobe periodic with a wavelength λ in the transverse direction Z. Therefore, the disturbances superimposed on the two-dimensional basic flow quantities can be expressed as

$$\begin{aligned} &F(X,Y,Z) = F_b(X,Y) + f'(X,Y)\exp(ia'Z),\\ &W(X,Y,Z) = w'(X,Y)i\exp(ia'Z), \end{aligned} \quad (8)$$

where $F = U, V, P$ or T, $f' = u', v', p'$ or t' $\cdot$ $a' = 2\pi/\lambda$ is the dimensional transverse wave number of the vortex rolls. By a consideration of the vortex-type perturbation quantities in the continuity equation, a different expression for W is used.

Substituting Eq. (8) into the continuity, Navier–Stokes, and energy equations in Cartesian coordinates, and subtracting the two-dimensional basic flow and energy equations under the assumptions of $Gr_L \gg 1$, one can obtain the linearized perturbation equations.

$$\frac{\partial u'}{\partial X} + \frac{\partial v'}{\partial Y} - a'w' = 0, \quad (9)$$

$$U_b\frac{\partial u'}{\partial X} + u'\frac{\partial U_b}{\partial X} + V_b\frac{\partial u'}{\partial Y} + v'\frac{\partial U_b}{\partial Y} = g\beta(t' - T_\infty)\sin\phi - \frac{1}{\rho}\frac{\partial p'}{\partial X} + \nu\nabla^2 u', \quad (10)$$

$$U_b\frac{\partial v'}{\partial X} + u'\frac{\partial V_b}{\partial X} + V_b\frac{\partial v'}{\partial Y} + v'\frac{\partial V_b}{\partial Y} = g\beta(t' - T_\infty)\cos\phi - \frac{1}{\rho}\frac{\partial p'}{\partial Y} + \nu\nabla^2 v', \quad (11)$$

$$U_b\frac{\partial w'}{\partial X} + V_b\frac{\partial w'}{\partial Y} = -\frac{1}{\rho}\frac{\partial p'}{\partial Z} + \nu\nabla^2 w', \quad (12)$$

$$U_b\frac{\partial t'}{\partial X} + V_b\frac{\partial t'}{\partial Y} + u'\frac{\partial T_b}{\partial X} + v'\frac{\partial T_b}{\partial Y} = \alpha\nabla^2 t', \quad (13)$$

where β is the coefficient of thermal expansion and $\nabla^2 = (\partial^2/\partial Y^2) - a'^2$ is a two-dimensional Laplacian operator. The perturbation equations are two-dimensional and of boundary layer flow-type.

Next, one introduces the following dimensionless variables and parameters:

$$\begin{aligned} &X = Lx, \quad [Y \quad Z] = LGr_L^{-1/5}[y \quad z],\\ &\begin{bmatrix} U_b & u' \end{bmatrix} = \frac{\nu}{L}Gr_L^{2/5}[\bar{u} \quad u], \quad \begin{bmatrix} V_b & v' & w' \end{bmatrix} = \frac{\nu}{L}Gr_L^{1/5}[\bar{v} \quad v \quad w],\\ &\begin{bmatrix} T_b - T_\infty & t' \end{bmatrix} = (T_w - T_\infty)[\theta_b \quad t], \quad p' = \frac{\rho\nu^2}{L^2}Gr_L^{4/5}p,\\ &a' = \frac{Gr_L^{1/5}}{L}a,\\ &Gr_L = \frac{g\beta(T_w - T_\infty)L^3}{\nu^2}, \end{aligned} \quad (14)$$

and a vorticity function in the axial direction

$$\xi = \frac{\partial w}{\partial y} - \frac{\partial v}{\partial z} = \frac{\partial w}{\partial y} - av. \quad (15)$$

To obtain equation for the vorticity, one may differentiate Eqs. (11) and (12) by z and y, respectively, and then eliminate the pressure terms by subtracting one from another. To derive the equation for v, one may differentiate Eq. (15) with respect to z. Similarly, the equation for w can be obtained by differentiating Eq. (15) by y. It is noted that in the derivation of equations for v and w, the continuity Eq. (9) must be considered. By also using the similarity variable $\eta = y/x^{2/5}$, the perturbation equations in η and x plane are found:

$$\frac{\partial^2 u}{\partial\eta^2} + \left(\frac{3}{5}f + x\frac{\partial f}{\partial x}\right)\frac{\partial u}{\partial\eta} - xf'\frac{\partial u}{\partial x} - \left(\frac{1}{5}f' + a^2x^{4/5} + x\frac{\partial f'}{\partial x} - \frac{2}{5}\eta f''\right)u = f''x^{3/5}v + Gr_L^{1/5}x^{4/5}t\sin\phi, \quad (16)$$

$$\frac{\partial^2 t}{\partial\eta^2} + \left(\frac{3}{5}f + x\frac{\partial f}{\partial x}\right)Pr\frac{\partial t}{\partial\eta} - xf'Pr\frac{\partial t}{\partial x} - a^2x^{4/5}t = x^{-1/5}Pr\frac{\partial\theta_b}{\partial\eta}\left(-\frac{2}{5}\eta u + x^{3/5}v\right) + Prux^{4/5}\frac{\partial\theta_b}{\partial x}, \quad (17)$$

$$\frac{\partial^2\xi}{\partial\eta^2}+\left(\frac{3}{5}f+x\frac{\partial f}{\partial x}\right)\frac{\partial\xi}{\partial\eta}-xf'\frac{\partial\xi}{\partial x}-\left(\frac{2}{5}\eta f''+a^2x^{4/5}-\frac{1}{5}f'-x\frac{\partial f'}{\partial x}\right)\xi=x^{4/5}Gr_L^{2/5}at\cos\phi-au\left(\frac{1}{25x^{3/5}}(6f-2\eta f'-8\eta^2f'')\right)+\frac{1}{5}x^{2/5}\left(4\eta\frac{\partial f'}{\partial x}-6\frac{\partial f}{\partial x}\right)-x^{7/5}\frac{\partial^2 f}{\partial x^2}\right)+x^{3/5}f''\left(\frac{\partial w}{\partial x}-\frac{2\eta}{5x}\frac{\partial w}{\partial\eta}\right), \tag{18}$$

$$\frac{\partial^2 v}{\partial\eta^2}-x^{4/5}a^2v=ax^{2/5}\xi-x^{2/5}\frac{\partial^2 u}{\partial x\partial\eta}+\frac{2}{5}x^{-3/5}\eta\frac{\partial^2 u}{\partial\eta^2}+\frac{2}{5}x^{-3/5}\frac{\partial u}{\partial\eta}, \tag{19}$$

$$\frac{\partial^2 w}{\partial\eta^2}-x^{4/5}a^2w=x^{2/5}\frac{\partial\xi}{\partial\eta}-ax^{4/5}\frac{\partial u}{\partial x}+\frac{2}{5}ax^{-1/5}\eta\frac{\partial u}{\partial\eta}. \tag{20}$$

The above equations are in x–η plane instead of x–y plane. The η axis covers all the variations of main flow in the x–y plane and probably most of the variations of perturbation quantities. Therefore, the computation time for solving Eqs. (16)–(20) may be much shorter than that for equations in the x–y plane. The set of equations (16)–(20) is a boundary value problem in the η-direction, an initial value problem in the x-direction, and an eigenvalue problem in the z-direction. This type of formulation and approach completely abandons the conventional approach in seeking an undefined solution with fixed zero or other finite values of x-derivatives. The growth of the magnitude of longitudinal vortices is part of the solution. The appropriate initial condition and boundary conditions of the perturbation equations are:

$$\begin{aligned} &u=v=w=t=0 \quad \text{at } \eta=0,\\ &u=v=w=t=\xi=0 \quad \text{at } \eta=\infty,\\ &u=v=w=\xi=t-t^0=0 \quad \text{at } x=0. \end{aligned} \tag{21}$$

For simplicity, the initial amplitude function t^0 is set uniform, and the other velocity components u, v and w are set to zero. However, the magnitudes of the velocities u, v and w will be generated in the next x-steps. The magnitude of the initial amplitude function, $t^0=10^{-4}$ is used in the present study.

Eqs. (16)–(20) and boundary conditions (21) in the x–η plane are for unknowns u, t, ξ, v and w with two fixed values of a and Gr_L. By giving a series value of a, the largest amplification of the perturbation quantities along the x-direction determines the value of the critical wave number a^*. One may analytically prove the homogeneity of L for $\phi=0°$ in Eqs. (16)–(20) by considering the dimensionless transformations (14), i.e., $u\sim L^{-1/5}$, $v\sim L^{2/5}$, $w\sim L^{2/5}$, $a\sim L^{-2/5}$, $x\sim L^{-1}$, $y\sim L^{-2/5}$, $z\sim L^{-2/5}$, and $\xi\sim L^{4/5}$ (variables of η and f are independent of L). In the computation, the selection of Gr_L does not change the local critical Grashof number Gr_X^* and the critical wave number $(ax^{2/5})^*$. This is also proved by using several values of Gr_L in the computation. The present study, $Gr_L=10^8$ is used for demonstrating the results.

The local Nusselt number of the basic and perturbed flows can be also expressed as,

$$Nu_X=Nu_b+Nu_p=\frac{(h_b+h_p)X}{k}=-Gr_X^{1/5}\left[\theta_b'(x,0)+\left.\frac{\partial t(x,0)}{\partial\eta}\right|_w\right]$$

or

$$\frac{Nu_X}{Nu_b}=\left[1+\left.\frac{\partial t(x,0)}{\partial\eta}\right|_W\Big/\theta_b'(x,0)\right], \tag{22}$$

where h is the local heat transfer coefficient, the subscripts b and p indicate the basic and perturbed flows, and k is the fluid thermal conductivity. It is noted that Nu_X is based on the thermal boundary condition of the constant wall temperature.

3. Numerical procedure

A finite difference scheme based on the weighting function [10] with second-order accuracy in both η and x is used. The step-by-step procedure is listed as follows:

1. Assign Pr, Gr_L and ϕ to obtain the basic flow and temperature distributions. The value of Pr is 0.7 (for air) and 7.0 (for water), $Gr_L=10^8$, and the values of ϕ are 0°, 5°, 10°, 15°, 20°, 30°, 45°, 60°, and 70°.
2. Assign zero initial values of u, v, w, and ξ, the initial temperature at the leading edge, $t^0=10^{-4}$ and various values of the wave number a.
3. Solve Eqs. (17)–(19) for u, t and ξ distributions at the next x-step. Values of ξ on the boundary are evaluated with the previous iteration data of v and w in the interior region.
4. Solve Eqs. (20) and (21) for v and w with the obtained u and ξ.
5. Repeat steps 3 and 4, until the perturbation quantities meet the convergence criteria at the streamwise position
$$\mathrm{Max}\left(\frac{\left|F_{i,j}^{(n+1)}\right|-\left|F_{i,j}^{(n)}\right|}{F_{i,j}^{(n+1)}}\right)\leqslant 10^{-5},$$
where $F_{i,j}^{(n)}$ are the perturbation quantities u, v, w, t and ξ of the nodal point (i,j) at the nth number of iteration.
6. Calculate the local Nusselt number of the vortex flow.

Table 1
Grid size test for $Gr_L = 10^8$, $a^* = 1.6$, $Pr = 0.7$ and $\phi = 0°$

η_∞	Δx	$\Delta\eta$	$x = 0.04$	0.08	0.12	0.14	0.16
10	0.002	0.02	0.01821[a]	7.240	78.66	955	123×10^2
10	0.002	0.01	0.01818	7.180	77.18	941	121×10^2
10	0.001	0.02	0.01818	7.172	77.10	938	119×10^2
15	0.002	0.02	0.01818	7.178	77.14	940	120×10^2

[a] These are the maximum values of the perturbation temperature $t/0.01$ at the specified x position.

7. Repeat steps 3–6, at the next mainstream position until a desired mainstream position is reached.
8. The absolute values of perturbation quantities grow along the mainstream direction. One can find the mainstream position marked with x_{cr}, where the onset criterion $Nu_p/Nu_b = 0.1$ is satisfied. Various onset positions x_{cr} can be determined for different values of the wave number a. The minimum x_{cr} denoted by x^* is the most probable onset position and the corresponding wave number is denoted by a^*. The local critical value is $Gr_X^* = Gr_L x^{*3}$ and the local wave number is $a^* x^{*2/5}$ for this computation.

The criterion for the determination of the onset of longitudinal vortices using the technique of heat transfer measurement in experiments can be explained as follows:

It was known that heat transfer rate can be increased by introducing a secondary flow. The onset position can be determined by a comparison of the heat transfer rate between the measured values of secondary flow and the basic flow data (6–30% of Nu_p/Nu_b by Incropera et al. [11], 15% of Nu_p/Nu_b by Maughen and Incropera [12], 10% of Nu_p/Nu_b by Chou and Han [13], etc.). Also, by a comparison of the onset criterion between $Nu_p/Nu_b = 0.2$ and $Nu_p/Nu_b = 0.1$ in the numerical experiment, the values of the onset position x^* increases by less than 4%. It is reasonable to set $Nu_p/Nu_b = 0.1$ for the onset criterion of longitudinal vortices in the numerical solution by heat transfer measurement techniques.

The grids tested for various Δx, $\Delta\eta$ and η_∞ are listed in Table 1. A grid size of $\Delta x = 0.002$, $\Delta\eta = 0.02$ and $\eta_\infty = 10$ is used to perform the numerical experiment in the present study. To check the validity of the linear equations (16)–(20), the order of magnitude of the nonlinear terms of perturbation equations near the onset position are checked. The calculated data are substituted into the individual terms of the x-momentum equation. The orders of the nonlinear terms is two orders of magnitude less than the order of linearized inertia terms. Therefore, the linear theory is valid for the estimation of the onset of longitudinal vortices in a laminar natural convection flow over horizontal and inclined heated plates.

4. Results and discussion

A typical development of the dimensionless perturbation amplitudes u, v, w, and t at $x = 0.1$, 0.12, and 0.14 for $Pr = 0.7$, $Gr_L = 10^8$, $a^* = 1.6$, and $\phi = 0°$ is shown in Fig. 2. The magnitudes of v and w are larger

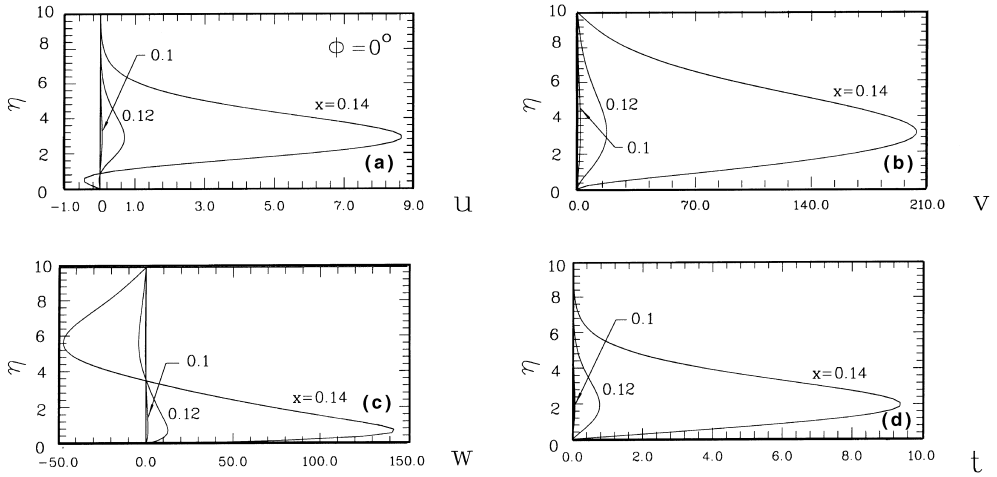

Fig. 2. Development of perturbation amplitude profiles at specified x positions for $\phi = 0°$ and $Pr = 0.7$.

than those of u and t because the scaling factor $(L/v)Gr_L^{-1/5}$ is included in these quantities. The shapes of the v and w profiles may be regarded as a vortex pattern. It is noted that a reversed velocity profile near the wall was induced downstream of the linear development region of the longitudinal vortices.

Fig. 3 depicts the dimensionless perturbation amplitude functions at $x = 0.24,\ 0.26$ and 0.28 with the value of the inclined angle $\phi = 30°$. It is seen that the values of perturbation amplitude functions are decreased with the stabilizing effect of the increased inclined angle ϕ. It is also observed in this figure that the profiles of perturbation amplitude functions are shrunk to the smaller η region due to the angle effect.

It is also interesting to study numerically the variations of local heat transfer rate after the onset of longitudinal vortices. The perturbation heat transfer rate Nu_p behaves like a cosine function in the Z-direction (i.e., $Nu \propto (\partial T/\partial Y) \propto \exp(ia'Z)$). Although the mean values of heat transfer rate in one spanwise wave are zero, the maximum variation of local heat transfer rate along z-direction occurred at $z = 0$ and $z = 2\pi/a$. The variations of local Nu_X/Nu_b along the axial direction at $z = 0$ are shown in Fig. 4. The correlation equation for the turbulent-free convection for the horizontal plate is also shown for comparison [14,15], i.e.,

$$Nu_X = 0.13(Pr\,Gr_X)^{1/3}$$

or

$$\frac{Nu_X}{Nu_b} = \frac{0.13(Pr\,Gr_X)^{1/3}}{0.3545Gr_X^{1/5}} = 0.3256Gr_X^{2/15}, \tag{23}$$

where $\theta'_b(X,0) = 0.3545$ at $\phi = 0°$ and $Pr = 0.7$ is chosen for reference.

The gradients of the temperature at the wall start to deviate from the laminar natural convection at downstream of x^*, due to the secondary longitudinal vortex flow on the heated plate. The angle effects on the longitudinal vortices are less pronounced when the values of the inclined angle ϕ increases.

The physical meanings of the critical values of Gr_X^*, and the local critical wave number $a^*x^{*2/5}$ can be interpreted as follows: they may be converted to $Gr^*_{\delta_r}$ and $a'^*\delta_r$, respectively, by the following transformations:

$$Gr^*_{\delta_r} = Gr_X^{*2/5}, \quad \left(a'\delta_r\right)^* = \left(\frac{2\pi}{\lambda}\frac{X}{Gr_X^{1/5}}\right)^* = \left(ax^{2/5}\right)^*, \tag{24}$$

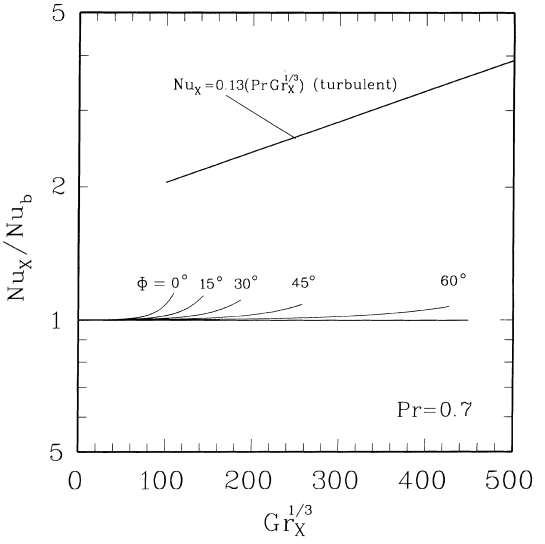

Fig. 4. Nusselt number vs. Grashof number.

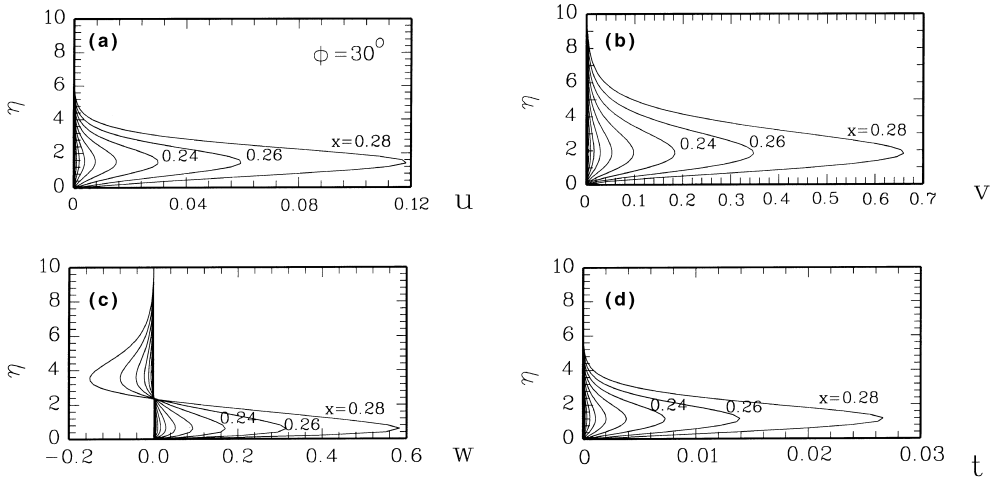

Fig. 3. Development of perturbation amplitude profiles at specified x positions for $\phi = 30°$ and $Pr = 0.7$.

Table 2
Onset position x^* for criterion $Nu_p/Nu_b = 0.1$[a]

ϕ (deg)	$Pr = 0.7$ ($a^* = 1.6$)			$Pr = 7.0$ ($a^* = 4.8$)		
	x^*	$Gr^*_{\delta_r}$	$a'^*\delta_r$	x^*	$Gr^*_{\delta_r}$	$a'^*\delta_r$
0	0.098	97.6	0.632	0.026	19.9	1.11
5	0.118	121.9	0.680	0.034	27.4	1.24
10	0.142	152.2	0.733	0.044	37.3	1.38
15	0.170	189	0.788	0.056	49.9	1.52
20	0.206	238	0.850	0.070	65.2	1.66
30	0.298	371	0.986	0.108	110	1.97
45	0.524	730	1.24	0.198	227	2.51
60	1.038	1646	1.62	0.410	544	3.36
70	1.998	3623	2.11	0.888	1374	4.58

[a] Values are evaluated by using $Gr_L = 10^8$ and $t^0 = 10^{-4}$.

where the local boundary layer characteristic thickness $\delta_r = X/Gr_X^{1/5}$.

The effect of inclined angle ϕ on the critical Grashof number $Gr^*_{\delta_r}$ is listed in Table 2. It is observed from the data that an increase in the inclined angle ϕ increases the value of the critical Grashof number $Gr^*_{\delta_r}$. The flow is more stable due to a decrease in the buoyancy force in the normal direction. Figs. 5 and 6 summarize the results of the present and previous works on the thermal instability in natural convection boundary layers. It is seen in Fig. 5 that there is a significant difference of one to two orders in magnitude between the experimental data and the previous theoretical prediction by using the nonparallel flow model and considering $(\partial/\partial\eta)_x \gg (\partial/\partial x)_\eta$ [8,16]. It is shown in Fig. 6 that the Prandtl number has a destabilizing effect on the flow and the critical values of the Grashof number decrease with an increase in the Prandtl number. The experimental data of Tollmien–Schlichting wave mode for $\phi > 70°$ are also shown for comparison. The results of the present study show a reasonable agreement with the previous experimental results [17–20].

In the above analysis, three sets of parameters are used. The three sets of parameters are summarized and discussed as follows. First of all, x^* and a^* are sought by using fixed Pr and Gr_L. Secondly, x^* and a^* are converted to Gr^*_X and $a^*x^{*2/5}$. Finally, $Gr^*_{\delta_r}$ and $(a'\delta_r)^*$ are used. The first set of parameters mainly comes from the length scale of plate. The second set of parameters considers the buoyancy to viscous force ratio of the boundary layer. The third set of parameters is derived from the characteristic thickness of the boundary layer.

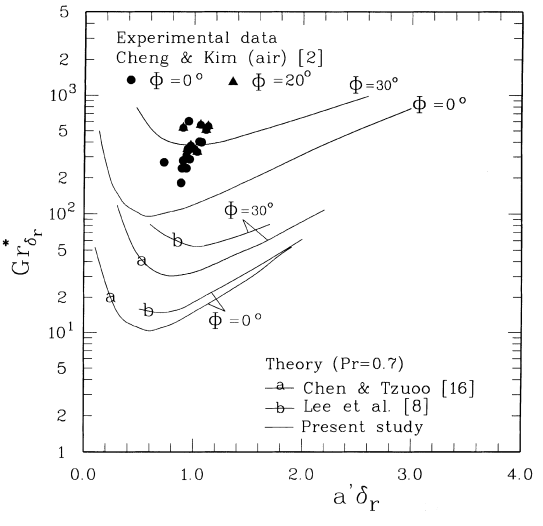

Fig. 5. Relation between the critical values $Gr^*_{\delta_r}$ and wave number $a'^*\delta_r$.

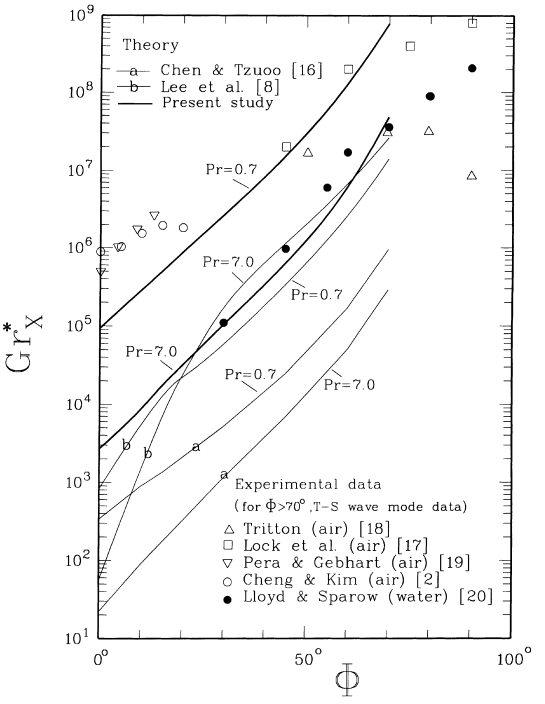

Fig. 6. Critical Grashof number vs. inclined angle ϕ.

5. Conclusions

1. The effect of the inclined angle from the horizontal on the stabilization of the thermal instability in natural convection boundary layers is studied numerically by using the heat transfer rate onset criterion and a linear instability model.
2. An increase in the inclined angle ϕ increases the value of the critical Grashof number Gr_X^*. The flow is more stable due to a decrease in buoyancy force in the normal direction. The effects of inclined angle on the Nusselt number are less pronounced when the values of the inclined angle ϕ increase.
3. The Prandtl number has a destabilizing effect on the flow and the critical values of the Grashof number decrease with an increase in the Prandtl number. The results of the present study show a reasonable agreement with the previous experimental data.

Acknowledgements

The author would like to acknowledge the National Science Council of ROC for its financial support for the present work through the project NSC 89-2212-E-233-002. This paper is also dedicated to Professor G.J. Hwang, Department of Power Mechanical Engineering, National Tsing-Hwa University, Hsinchu, Taiwan, ROC.

References

[1] E.M. Sparrow, R.B. Husar, Longitudinal vortices in natural convection flow on inclined surfaces, J. Fluid Mech. 37 (1969) 251–255.
[2] K.C. Cheng, Y.M. Kim, Flow visualization studies on vortex instability of natural convection over horizontal and slightly inclined constant temperature plate, ASME J. Heat Transfer 110 (1988) 608–615.
[3] E.J. Zuercher, J.W. Jacobs, C.F. Chen, Experimental study of the stability of boundary layer flow along a heated, inclined plate, J. Fluid Mech. 367 (1998) 1–25.
[4] G. Evan, R. Grief, A study of traveling wave instabilities in a horizontal channel flow with application to chemical vapor deposition, Int. J. Heat Mass Transfer 32 (5) (1989) 895–911.
[5] F.P. Incropera, Convective heat transfer in electronic equipment cooling, ASME J. Heat Transfer 110 (1988) 1097–1111.
[6] S. Sathe, B. Sammakia, An review of recent developments in some practical concepts of air-cooled electronic packages, ASME J. Heat Transfer 120 (1998) 830–839.
[7] B. Gebart, Y. Jaluria, R.L. Mahajan, B. Sammakia, Buoyancy-induced flows and transport, Hemisphere (1988) 633–640.
[8] H.R. Lee, T.S. Chen, B.F. Armaly, Nonparallel thermal instability of natural convection flow on non-isothermal inclined flat plates, Int. J. Heat Mass Transfer 35 (1) (1992) 207–220.
[9] G.J. Hwang, M.H. Lin, Estimation of the onset of longitudinal vortices in a laminar boundary layer heated from below, ASME J. Heat Transfer 117 (1995) 835–842.
[10] S.L. Lee, Weighting function scheme and its application on multidimensional conservation equations, Int. J. Heat Mass Transfer 32 (11) (1989) 2065–2073.
[11] F.P. Incropera, A. Knox, J.R. Maughen, Mixed convection flow and heat transfer in the entry region of a horizontal rectangular duct, ASME J. Heat Transfer 109 (1987) 434–439.
[12] J.R. Maughen, F.P. Incorpera, Experiments on mixed convection heat transfer for airflow in a horizontal and inclined channels, Int. J. Heat Mass Transfer 30 (7) (1987) 1307–1318.
[13] F.C. Chou, C.S. Han, Wall conduction effect on the onset of thermal instability in horizontal rectangular channel, Exp. Heat Transfer 4 (1991) 355–365.
[14] T. Fujii, H. Imura, Natural convection heat transfer from a plate with arbitrary inclination, Int. J. Heat Mass Transfer 15 (4) (1972) 755–767.
[15] K.C. Cheng, T. Obata, R.R. Gilpin, Buoyancy effects on forced convection heat transfer in the transition regime of a horizontal boundary layer heated from below, ASME J. Heat Transfer 110 (1988) 596–603.
[16] T.S. Chen, K.L. Tzuoo, Vortex instability of free convection flow over horizontal and inclined surfaces, ASME J. Heat Transfer 104 (1982) 637–643.
[17] G.S.H. Lock, C. Gort, G.R. Pond, A study of instability in free convection from an inclined plate, Appl. Sci. Res. 18 (1967) 171–182.
[18] D. Tritton, Transition to turbulence in the free convection boundary layers on an inclined heated plate, J. Fluid Mech. 16 (1963) 417–435.
[19] L. Pera, B. Gebhart, On the stability of natural convection boundary layer flow over horizontal and slightly inclined surfaces, Int. J. Heat Mass Transfer 16 (6) (1973) 1147–1163.
[20] J.R. Lloyd, E.M. Sparrow, On the instability of natural convection flow on inclined plates, J. Fluid Mech. 42 (1970) 465–470.